Developing a FRET-based Activation Indicator in Ste2p, a Yeast GPCR

A Major Qualifying Project submitted to the faculty of Worcester Polytechnic Institute in partial fulfillment of the requirements for the Degree of Bachelor of Science

Submitted by:

Victoria Johnson

Project Advisors:

Destin Heilman (WPI)

Mark Dumont (URMC)

Sara Connelly (URMC)

April 26th, 2018

Abstract

Of great interest to the pharmaceutical market, G protein coupled receptor (GPCR) behavior is still not well understood. The interplay between ligand binding, receptor activation, and the resulting cellular response is not well categorized. Current assays to measure activation are indirect and rely on downstream activation of reporter genes. Successful in other GPCRs, a FRET-based direct indicator of activation was developed in Ste2p, a member of the yeast mating pheromone response pathway. The current system could be successful but some improvements could make the indicator more versatile in its application. Identification of a successful clone will allow further studies of GPCR behaviors, such as fractional occupancy. Pharmaceutical dosing of GPCR-targeted medicines relies on understanding the dynamic relationship of binding, activation, and output that impacts receptor behavior.

Table of Contents

Acknowledgements

I would like to recognize and thank several people for their support and guidance during the course of this project:

Destin Heilman, for agreeing to be my advisor and allowing me to complete this project remotely. His flexibility allowed me to finish the last aspect of my degree and complete my goal of graduation, even if it took a little longer than I expected.

Mark Dumont, for graciously allowing me to join his lab at the University of Rochester Medical Campus, his scientific guidance, and help interpreting results. He provided me the opportunity to finish my degree requirements in a supportive and collaborative laboratory environment.

Sara Connelly, for all of her professional and personal guidance, oversight, and support. Her mentorship helped me learn how to work with yeast and develop experiments. I could not have completed this project without the foundation she helped me build. Her personal counseling and understanding helped me thrive in the laboratory. Ultimately, her instruction and direction are immeasurable and I will be forever grateful.

Liz Mathew and Hong Zhu, for making the laboratory environment comfortable and supportive. Their positive attitudes and hijinks brought a light and pleasurable setting to the lab. Their work on an HIV vaccine taught me about the trials and tribulations that research entails.

Kyle Morrison, for his late night chats about life, optimism during the thick of it, and technical writing support. He provided a guiding hand with never ending comments to help shape push my project toward its true potential. His friendship during this difficult period helped me not give up on myself. The support he has given me deserves more recognition than I could ever give in words.

Background

Signal transduction within and between cells is imperative for the survival of all organisms. Propagation of a signal is dependent on receptors that occupy the cell surface to accept external messages and relay them into the cell. Containing over 800 different cell surface receptors, the G protein-coupled receptor (GPCR) superfamily plays an integral part in signal transduction and overall cell homeostasis (Tang et al 2012). This superfamily has become one of the most studied protein families, especially due to extensive genome sequencing of various organisms from plants to humans. As membrane proteins, GPCRs contain long hydrophobic stretches which make crystallization and other structural studies difficult. The first GPCR to be crystallized was rhodopsin in 2000 (Palczewski et al). GPCRs contain seven transmembrane (TM) helices and respond to a diverse collection of stimuli including photons, odorants, lipids, hormones, neurotransmitters, and other small molecules. Composing around 3% of the human genome, GPCRs are culprits of many disease states and the target of many pharmaceuticals (Fredriksson & Schiöth 2005). Continued research is essential to further understand the structure, mechanisms, and behaviors of GPCRs to optimize pharmaceutical efficacy.

GPCRs are present in every cell of the human body as well as in a majority of other organisms. Many human disease states, can be attributed to incorrect autoimmune targeting of GPCRs and, less frequently, receptor mutations. Because of the diverse nature of GPCRs, a wide range of disease states have been associated with the incorrect autoimmune targeting of these surface receptors; diseases including, but not limited to, hormonal disruptions, metabolic diseases, and many psychiatric disorders (Insel et al 2007). There is also significant evidence of GPCR activity in tumorigenesis and cancer progression (Gutierrez & McDonald 2018). Their diversity has made GPCRs become the target of around 36% of pharmaceuticals on the market today (Rask-Andersen, Almen, & Schioth 2011)**.**

For many GPCRs, endogenous agonists and antagonists have been identified; however, roughly 15% are considered “orphan receptors,” with no known ligands (Insel et al 2007). Current pharmaceutical research focuses on de-orphanization in order to gain a broader knowledge about the relationship between ligand binding, receptor activation, and cellular responses in GPCRs. The interplay between binding, activation,

and response, is the basis for regulate the dosage of pharmaceuticals that target these receptors and the myriad of disease states associated.

Understanding this dynamic relationship relies on information about the basic structure, behavior, and cellular responses induced by GPCRs. Few crystal structures have been completed of these surface receptors, however the basic structure for all GPCRs contain seven hydrophobic helical transmembrane structures with major differences occurring mainly in the extracellular loops (Rosenbaum, Rasmussen, & Kobilka 2009). The amino-terminus of the protein extends into the extracellular matrix and impacts receptor functionality and expression levels at the cell surface (Uddin et al 2015). There is also a significant carboxyl-terminus tail extending into the cytoplasm which is believed to have negative regulatory roles on signaling and to be important for receptor/G protein interactions; removing or modifying the C-terminus leads to constitutive activity and decreased internalization of receptors (Kim et al 2011).

On the cytoplasmic side, these receptors are associated with a heterotrimeric G protein consisting of alpha, beta, and gamma subunits. There is evidence to support pre-coupling and pre-assembly is present for GPCRs and their associated G proteins (Hein & Bünemann 2009, Cevheroğlu, Becker, & Son 2017), it is not well understood if pre-assembly is the steady state or only if it is only initiated by ligand binding. Pre-coupling would ensure a GPCR is primed for any environmental changes it may encounter to produce the appropriate cellular response. Given the diversity of GPCRs and the range of possible stimuli, a quick response is essential for cellular and organism survival.

During activation, conformational changes occur within the receptor and within the heterotrimeric G protein bundle. In the yeast model system, it is believed that upon activation by a ligand, transmembrane helices 5 and 6 have a slight shift toward one another, thus initiating the intracellular signal transduction cascade (Kobilka 2007, Taslimi et al 2012). Next, Gα is activated, an exchange of GDP for GTP occurs, and the Gβ/Gγ subunits are released (Bardwell 2004). Full dissociation of the heterotrimer is not believed to occur, but a rearrangement of the subunits is sufficient for signal transmission (Bünemann, Frank, & Lohse 2003). The free Gβ/Gγ subunits initiate a three-tiered protein kinase cascade ending with transcription modulation of multiple genes (Bardwell 2004). Transcription, the primary cellular response, occurs after a long

chain of events from the initial ligand messenger. This cellular response can be easily monitored through use of reporter genes such as β-galactosidase induction (Yan et al. 2002). Restoration of β-gal indicates an active receptor, or positive signal. This assay, however, does not give a direct conformation of receptor activation by a ligand; but, it only provides evidence of a cellular response occurring. Mammalian GPCRs have slightly different protein interactions, however, the general behavior translates between systems. Expression of homologous human GPCRs is possible within the yeast system with only minor modifications of interacting proteins (Liu, Wong, & IJzerman 2016).

Previously considered a simple on/off switch with one active conformational state and one inactive state, GPCRs actually have complex activation and signaling responses to a variety of agonists and antagonists. Activation was once believed to behave as direct relationship between agonist or antagonist bound and concentration of receptors present. This theory would see the maximal response only from a cell containing a high concentration of receptors-agonist complexes and a low concentration of antagonist occupancy. However, in the presence of an antagonist, yeast cells actually require lower concentrations of agonist to achieve the maximal cellular response; the cellular signaling response to an agonist increases when empty receptors are occupied by antagonist (Sridharan et al 2016). Sridharan et al also found that the cellular signaling response decreases as more receptors become available at the surface (2016). Maximal signaling from the cell is not dependent on an absolute number of activated receptors, but instead follows a “fractional occupancy” behavior (Sridharan et al 2016, Bush et al 2016). Fractional occupancy suggests that once a threshold is met, a maximal cellular response can be triggered, even with minimal concentrations of receptors on the surface.

It can be implied that the receptor adopts a different conformational shape when activated by different agonists (Sridharan et al 2014). Partial agonists have been found for GPCRs that induce different conformational changes than full agonists in the same receptor (Swaminath et al 2005). Partial agonists are relevant and readily used in the pharmaceutical industry to create subtle corrections and, unlike full agonist medications, exposure does not lead to receptor desensitization as quickly (Bosier & Hermans 2007). The ability of receptors to adopt differential conformational shapes and produce different downstream cellular signaling responses for a variety of ligands is the foundation of

“biased agonism” (Kenakin 2007). A single receptor, dependent on ligand binding, is capable adopting multiple conformational shapes which can each activate a different cellular responses.

Much of the information known about GPCRs has been elucidated utilizing fluorescent labeling techniques including fluorescence spectroscopy, bimolecular fluorescence complementation (BiFc), fluorescence resonance energy transfer (FRET), bioluminescent RET, and fluorescein arsenical hairpin (FlAsH) reagents (Zimmermann et al 2002, Hoffman et al 2005, Kredel et al 2009, Kam et al 2012, Sridharan et al 2013, Kauk & Hoffman 2018). These techniques have helped elucidate aspects such as protein-protein interactions, binding site dynamics, and signaling output behaviors. Both ligands and receptors can be labeled using whole fluorescent proteins or small fluorescent molecules (Rajashri et al 2014). These fluorescent techniques are and will continue to be a crucial aspect in understanding the dynamic interplay between ligand binding, receptor activation, and cellular response strength; the underlying relationship that dictates dosing of GPCR-targeted pharmaceuticals.

Mammalian cells express a multitude of GPCRs simultaneously, each with the ability to induce a variety of cellular responses. To make the process of understanding GPCRS feasible, a simple, easily manipulated system is crucial for reproducible experiments and exploration. Unlike complex mammalian systems, yeast cells contain only two GPCRs during the haploid stage and only three while diploid (Bardwell 2007). The standard model yeast system, *Saccharomyces cerevisiae*, contains only 6,000 genes that have been completely sequenced (Goffeau et al 1996). Full genome sequencing has allowed for straightforward manipulation and elimination of genes, as well as generation of mutant yeast strains containing desired genetic modifications allowing for complete control over the intracellular environment. The most well characterized yeast GPCR is Ste2, a member of the yeast mating pheromone response pathway (Bardwell 2007). Produced by MATa haploid yeast cells, the Ste2 receptor is activated by α-factor produced by the opposite mating type, MATα cells. Ste2 deletions from the genome and reintegration via plasmids under different promoter controls or after mutagenesis are possible.

Specific receptor activation is important in understanding the relationship between binding of ligand, receptor activation, and cellular response; the relationship is the basis of the dosing curve utilized in pharmaceuticals and therefore must be understood. This project aims to concentrate on developing an activation assay that is specific and direct indication of receptor activation. Differential activation states by different ligands could be identified by this proposed activation assay. This project aims to develop a system to identify receptor activation instead of relying on a downstream effector to signal a positive response. A receptor that contained a fluorescent indicator would allow direct observation of activation and could be used in future experiments to better understand the GPCR dosing curve. This project utilized the receptor system Ste2 in yeast and was completed in the lab of Mark Dumont at the University of Rochester. A pair of fluorophores would be used to identify intramolecular Förster resonance energy transfer (FRET). A positive library isolate would be able to identify conformational changes associated with receptor activation directly. This project worked to identify factors that affect fluorescent signal strength of the Ste2 receptor system and to optimize detection of FRET activity.

Methods

Strains Used

The yeast strain A575 was used as the background for all experimentals, containing STE2, FAR1, BAR1, URA, and LEU deletions. Plasmids pMD1154 or pMD1167 containing URA+, ampicillin resistance gene (amp-R), and wild type truncated or full length STE2 with GFP[2], were used to create strains A4242 and A4243, respectively. The library, Ste2p with mRuby[2] and GFP[2], was created in the background strain A575 with mutagenized plasmids pMD1154 or pMD1167 to form libraries L1858 and L1859, containing truncated or full length Ste2p, respectively. A negative control strain, A1239, was created from A575 containing an empty URA+ plasmid. A positive mRuby[2] control strain, A4971, was used containing an mRuby[2] labeled G protein α subunit, Gpa1p. A strain, A4793, containing a plasmid with amp-R present was used as a miniprep and transformation control.

Library Generation

The creation of the mutagenized library was completed by Sara Connelly according to the protocol developed previously in the Dumont Lab by Mathew et al. then frozen down. The mRuby[2] gene encoded on pMD2519 was amplified via PCR using primers ON1868 and ON1869 to introduce Bbs1 restriction sites to the 5’ and 3’ ends, respectively. Digestion by BbsI occurred before ligation to IC3 variable-length linkers on both the N- and C-termini. Plasmids pMD1167 containing full-length and pMD1154 containing truncated versions of the STE2 gene with BbsBI restriction sites and a C-terminus tail GFP[2] tag, were digested to delete the native IC3 loop. Both the mRuby-IC3 linker products and the plasmids were then subjected to gel purification before being mixed together, incubated, and used to transform NOVABlue cells and create libraries L1858 and L1859. A schematic of this protocol can be found in Appendix Figure 1.

Colony Growth and Maintenance

All yeast strains were grown on synthetic complete dextrose minus uracil (SD-ura) media on petri plates at 30℃for 48 hours. All plates were stored at 4℃after incubation time. From the freezer, yeast were grown, then single colonies were picked and streaked fresh, again single colonies were picked and master plates were produced. Master plates were remade every 3 weeks.

From master plates, colonies were grown in 4 mL of liquid SD-ura in 12 mL test tubes at 30℃ in a shaker until turbidity occurred. All cultures were stored at 4℃ after incubation time. Cultures were regrown to normalize growth rates based on optical density and Equation 1.

$$Inoculum\ Needed\ = \frac{Desired\ OD \times Culture\ Volume\ (mL) \times Conversion\ Rate\ (\frac{uL}{mL})}{2^{(Number\ of\ Doubling\ Times)} \times OD\ of\ Inoculum}$$

Equation 1: Inoculum needed to normalize cultures to a similar OD_{600}

Optical density was determined using a spectrophotometer at 600 nm (OD_{600}). Cultures were diluted 1:10 in SD-ura and a SD-ura blank was used to set the machine. Disposable cuvettes were filled with 1 ml of diluted sample and measurements were taken.

YPD/FOA Growth

Library isolates from L1858 and L1859 were overgrown in liquid yeast extract peptone dextrose (YPD) at 30°C for 48 hours. Aliquots of overgrown culture were diluted 1:1000 in ddH_2O, 25 µL of dilution was then plated with 150 µL of ddH_2O on both SD-ura and YPD using a spreader. Cultures were also overgrown in liquid SD-ura and plated in a similar fashion. After incubation, colonies on each plate were counted for comparison. Colonies from YPD grown/YPD plates, were replica plated onto FOA (ura- restrictive) plates using short fiber velveteen. YPD and FOA plates were placed in 30°C to establish fresh colony growth.

Fluorimeter

A spectrophotometer was used to find excitation and emission spectra of the GFP[2] within the yeast cells. Cultures of A1239 and A4242 were grown to an OD_{600} of 1 in SD-ura then diluted in phosphate-buffer saline (PBS) to an OD_{600} of 0.1 in quartz cuvettes with a stir bar for measurements. An excitation of 420 nm, emission range of 440-600 nm, slit width of 5 nm, 420/10 bandpass excitation filter, and a 450 long pass emission filter was used to measure the emission spectrum. An excitation range of 350-450 nm, an emission of 470 nm, slit width of 1 nm, no excitation filter, and a 470/10 bandpass emission filter was used to measure the excitation spectrum. Spectra were created by subtracting S_1/R_1 values of Raman peaks determined with ddH_2O from A4242 values. This was repeated for the mRuby[2] spectra using cultures of A5119. An excitation of 564

nm, emission range of 600-700 nm, slit of 10 nm, 560/10 band pass excitation filter, and a 600 nm long pass emission filter was used to measure the emission spectrum. An emission of 620 nm, excitation range of 500-600 nm, and 600 nm longpass emission filter was used to measure the excitation spectrum. Again values of Raman peaks were subtracted out.

Flow Cytometry

Samples grown to an OD_{600} of 1, containing 1.5 x 10^6 cells in 500 µL solutions of either PBS or SD-ura were examined utilizing two different LSR II analytical flow cytometers, Dr. Teeth (5 laser, 18 color) and Kermit (3 laser, 12 color). Strains A1239, A4242, A4242, L1858, and L1859 were grown to an OD_{600} of 1 and were normalized using the approximation that an OD_{600} of 1 is equal to 210^6 cells. Samples in SD-ura were run with and without addition of 50nM α-factor. Analysis of results were completed using the online software Cytobank.

Large streaks of colonies from Master plates of library isolates L1858-5 and L1859-5 were suspended in 420 µL of ddH_2O, enough to create turbidity. A variety of cultures were started with this suspension, aiming to reach a wide range of final optical densities. The ODs were measured and normalized to contain 1.5 x 10^6 cells in 500 µL of SD-ura. A1239, A4242, A4243, and A5119 were grown to OD_{600} 1 and normalized. Samples were then run through a LSR II analytical flow cytometer, Animal (5 laser, 18 color) and analyzed with Cytobank.

Western Blot

Samples from L1858, L1859, A1239, A4242, and A4243 were prepared containing $2x10^7$ cells, as done above, for Western blot analysis. Each pellet was suspended in 100µL of 1x protease inhibitor in Ste2 buffer containing Tris, EDTA, SDS, urea, and bromophenol blue. At 4°C, a 1 minute shake with zirconia/silica beads was followed by a 1 minute rest and repeated 5 times before the cells were spun down. The supernatants were collected and incubated for five minutes at 37°C. A 5% stacking, 12.5% resolving SDS-page acrylamide gel was then used for separation.

Transfer was completed using a nitrocellulose membrane in transfer buffer containing SDS, Tris, lysine, methanol and water, run overnight at a low voltage. A rinse with PBS

was followed by blocking through incubation with PBS, 5% newborn calf serum (NCS), and 0.1% tween. A series of washes with PBS and 0.1% tween was followed by a second incubation with 1:10,000 mouse anti-GFP in PBS and 5% NCS. Another series of washes with PBS, 5% NCS, and 0.1% tween was followed by a third incubation with 1:10,000 goat anti-mouse horseradish peroxidase in PBS, 5% NCS, and 0.1% tween. A final set of rinses was done in PBS and 0.1% tween before the membrane was prepped for imaging.

On a glass plate, the membrane was covered in 4 mL of Super Signal West Dura (50/50 peroxide buffer/luminol) for five minutes. The membrane was then dried and placed in a plastic sleeve. Film was exposed to the membrane for 5 seconds and then developed.

Yeast miniprep and E.coli transformation

Strains A1858 and A1859 were grown to an OD_{600} of 1, and used in two yeast miniprep kits, Zymoprep Yeast Miniprep II or Wizard Plus SV Miniprep DNA Purification System, to extract the plasmids. The Wizard protocol was modified for yeast plasmid extraction; enzymatic steps were skipped and replaced by vigorous shakes with zirconia/silica beads. A nanodrop spectrophotometer was used to verify DNA presence in the elutions. Plasmids were eluted in either 10 or 30 µL of ddH_2O, respectively, and added to 100 or 150 µL of competent E. coli cells. Cells were incubated on ice for an hour before heat shocked at 37°C for 45 seconds and then put on ice for 2 minutes. Cells were incubated with 1 mL of rich broth for an hour at 37°C. After a quick spin down, most of the supernatant was removed, then cells were resuspended and plated on YT media plus ampicillin using glass beads. Plates were incubated overnight at 30°C.

Microscopy

Strains L1858, L1859, A4242, A4243, and A1239 were grown to an OD_{600} of 0.4 overnight. 1 µL of culture was placed on a glass slide and covered by a glass coverslip. Cells were analyzed and imaged using an Olympus FV1000 laser scanning confocal microscope. GFP^2 and $mRuby^2$ were excited using the 405 nm and 560 nm laser, respectively. Images were also taken using the 488 nm laser to excited GFP^2.

Colony PCR (Supplemental Data)

Colonies were grown fresh on SD-ura plates and PCR was completed using Phusion High-Fidelity DNA Polymerase, 5’ ON458, and 3’ ON459 primers to flank the third intracellular loop in the transmembrane regions. Thirty-five cycles of 10 seconds at 98°C, 30 seconds at 55°C, then 30 seconds at 72°C were completed. PCR products were then ran on an agarose gel at 50V until separation occurred.

Results

GPCRs, because of their diversity and abundance, have become a large target for the pharmaceutical market. Effective dosing of GPCR-targeted medications relies on the elucidation of GPCR binding, activation, and cellular response behaviors. Continued research of GPCRs is crucial to understand their behavior. Current receptor activation research relies on reporter genes and downstream cellular responses, not direct receptor activation. An indicator of receptor activation, in real time, is key to for further studies of GPCR activation and signaling behavior. Use of the model system *S. cerevisiae* allows for a simple and controllable environment to study these behaviors which translate to more complex mammalian systems.

This project aimed to develop a direct indicator of GPCR activation through use of fluorescent resonance between two fluorophores. Conformational changes associated with receptor activation would cause changes in FRET intensity, by movement of the individual fluorophores. To create this readout system, a library was created containing mRuby^2 randomly inserted in the third intracellular loop of the yeast GPCR Ste2, which also had GFP^2 transcribed on the C-terminal tail. Two libraries were made in truncated and full length versions of Ste2 using a protocol developed previously in the Dumont lab by Mathew et al (2012). Individual clones were randomly chosen to investigate if the cells was producing the labeled receptor from the inserted plasmid and to optimize fluorescent detection. In order to identify a small shift in FRET activity upon activation in the receptor, detection and understanding how the system works first is a necessity.

An initial run on a 5 laser, 18 color LSR II flow cytometer (Dr.Teeth), was used to verify positive GFP^2 and empty vector controls. It was also used to identify the band pass filters required for detection of each fluorophore as well as FRET activity. Excitation by every laser and collection by every detector to select the best channels for analysis (data not shown). Excitation with the violet laser, 405 nm, was used to identify GFP^2 activity in the Violet E channel and transfer activity in the Violet D channel (Figure 2A and 2B). Analysis of this run using Cytobank found significant GFP^2 fluorescent activity from the positive, GFP^2 containing Ste2 controls (4242 and 4243), and only basal cellular fluorescence in the negative, empty vector control (1239), as expected. The six isolates randomly chosen for this run also showed a slightly higher fluorescent intensity than the empty vector, showing possible GFP^2 activity. No transfer activity was identified

in the Violet D channel in any of the library isolates. Excitation with the yellow-green (YG) laser, 561 nm, was used to identify mRuby^2 activity in both the YG E and YG D channels (Figures 2C and 2D). Both channels identified a high fluorescent intensity from the truncated isolates (1858) and slightly less, but still higher than basal activity in the full length isolates (1859). A strong mRuby^2 signal was identified over basal signaling, however, the GFP^2 intensity was not as significant. Truncated isolates consistently displayed brighter mRuby^2 activity compared to the full-length isolates.

As the libraries were created using random mutagenesis, some variation in fluorescent intensities was predicted. To see if stronger GFP^2 activity could be identified, 30 truncated isolates from L1858 were run on Dr.Teeth using the same lasers and channels as above. GFP^2 activity of the isolates were again slightly above basal fluorescence in the Violet E channel, but far below the intensity of the GFP^2 control (4242) (Figure 3A). Again, no transfer activity was detected in the isolates but mRuby^2 activity was abundant (Figures 3B-D). One isolate, 1858-A3, had activity inconsistent with the other isolates, more similar to the negative control in all channels. Some isolates, such as 1858-A1, C5, D3, and E3, showed slightly higher fluorescent intensities than the average in both the YG channels. Although these isolates displayed a stronger than average mRuby^2 signal, their GFP^2 activity did not have the same behavior. Quenching of GFP^2 by mRuby^2 activity would account for the lack of signal seen, however it is expected that this quenching would be identified by the Violet D channel. Without the identification of transfer activity, it is expected that GFP^2 and mRuby^2 would show similar intensities over basal signaling as they are at similar concentrations within the cells.

To verify GFP^2 production was present within the libraries, a Western Blot was performed under denaturing conditions, using randomly selected isolates as well as the bright isolates identified by the second Dr.Teeth run (Figure 4). Mouse anti-GFP primary antibodies with secondary goat anti-mouse antibodies conjugated to HRP were used to identify GFP^2; the anti-GFP antibody was not cross reactive with mRuby^2 (data not shown). A five second exposure of the membrane was used to get a clear image of the lanes without overexposing the film. Both mRuby^2 and GFP^2 have an expected weight around 26 kDa, full length Ste2 an expected weight around 48 kDa, and truncated Ste2 an expected weigh around 34 kDa, using the estimation that 33 amino acids have a

weight of 37 kDa**.** The full length control (Lane 1) and all L1859 isolates (Lanes 2-6) ran fairly clean with bands at their expected weights, 75 kDa and 100 kDa, respectively. All isolates had a band presence around 25 kDa, indicative of free GFP^2 cleaved from the receptor construct. Specifically, 1859-B2 had strong proteolytic behavior, showing two intense bands low on the blot and a less intense band at the expected 100 kDa area. Surface receptors often display smears on Western blots because of their membrane localization, however the truncated control (Lane 9) resulted in an unreadable blot. This could be caused by a high concentration of receptors as well. All L1858 isolates also are less clean than the full length isolates, but do show a band around the expected weight of 85 kDa. These isolates do not show significant proteolytic bands around 25 kDa, but do show intense bands of oligomerized receptors around 250 kDa. These bands are similarly present in the truncated isolates, but to a lesser extent. Band intensity overall is significantly higher in truncated isolates than the full length ones, supporting the intensity differences seen in the flow cytometry runs.

As proteolytic activity was evident in the Western blot, localization of the receptor construct was investigated. As Ste2p is a transmembrane GPCR, the construct is expected to be localized on the peripheral of the cell. Fluorophore presence within the cell would indicate endocytosis of receptors or proteolytic cleavage of the fluorophores in the lysosomes. Confocal microscopy was utilized to image cells expressing the Ste2-GFP^2 construct (A4242) and cells expressing a membrane localized protein-mRuby^2 construct (A5119) (Figure 5). Imaging of A4242 showed membrane localization of the GFP^2 as well as significant activity confined within the cell when excited at 488 nm (Figure 5A) and at 405 nm (data not shown). A portion of the cells seen under the bright field did not have any fluorescent activity. Imaging of A5119 was used as a positive mRuby^2 control at 561 nm; detection and imaging was not as strong or clear for mRuby^2 as it was for GFP^2 (Figure 5B). Cells containing mRuby^2, exposed to the 405 nm laser quickly experienced photo bleaching and became undetectable when imaged. Isolates of both L1858 and L1859 did not show detectable GFP^2 or mRuby^2 when imaged (Figure 5C); however, slight mRuby^2 activity could be seen through the ocular lens where photo bleaching could be watched over time. Stronger fluorescent intensities are required from the isolates if imaging of localization is desired.

After GFP^2 presence was confirmed within the library isolates by Western blot, further experiments to understand the plasmid and fluorescent behavior were conducted. Fluorimeter experiments were performed to identify the excitation and emission spectra of the fluorophores within the yeast cells. Identifying the true spectra of GFP^2 and mRuby^2 would allow for the optimization of detection of fluorophore activity and possible transfer activity in the future fluorimeter runs. Raman peaks were determined for the spectrophotometer using ddH_2O at each wavelength used. A positive GFP^2 control (A4242) was used to determine the GFP^2 spectra, subtracting out the Raman peak and basal cell fluorescence (A1239) to identify the signal strictly from the GFP^2 fluorophore (Figure 6A)***.*** The maximum excitation peak was seen at 410 nm, using an emission set at 518 nm. A Stokes' shift of about 100 nm was identified, with an emission peak at 510 nm which spanned from about 450 nm to 550 nm, when excited at 420 nm. mRuby^2 spectra were determined utilizing a positive control (A5119), basal fluorescence and Raman peaks were subtracted out as done for GFP^2 (Figure 6B). Maximal excitation occurred at 565 nm, when emission was set at 620 nm. A smaller Stokes' shift, of only 45 nm, was identified for mRuby^2 than GFP^2; an emission peak at about 610 nm which spanned from around 600 nm to 650 nm. Due to the 600 LP filter used for detection, the peak gets cut off at this point. Spectra were normalized to 100% of their own highest point for comparison of the overlap between fluorophores (Figure 6C). mRuby^2 excitation overlaps GFP^2 emission from around 525 nm to almost 600 nm. Isolates from both libraries were also analyzed at these wavelengths and a similar trend to flow data was seen: little GFP^2 activity with substantial mRuby^2 signal (data not shown). All samples were run with approximately 2 10^7 cells within the cuvettes; samples were concentrated to contain 610^7 cells and fluorescent peaks were more intense but peaks at the same wavelength (data not shown).

Fluorescent detection has posed a challenge due to low signal intensity. Identifying signal changes relies on maximizing signaling overall. It is known that overgrown cultures have increasing numbers of dead cells contributing to the OD that may no longer have strong fluorescent activity as well as increasing numbers of cells which has lost the plasmid of interest. To understand factors that may affect fluorescent behavior, experiments with optical density were conducted. A series of cultures from the same colony were grown to create a variety of OD_{600} ranging from 0.15 to 1.3. These samples were run on a 5 color, 18 laser LSRII flow cytometer (Animal), to identify differences in

fluorescent intensity (Figure 7). Visualizing differences through histograms alone was difficult (Figure 7A), however as a general trend, decreasing optical density resulted in increasing fluorescent mean intensity detected (Figure 7B). A similar trend was seen for full length cultures (data not shown). Optimizing fluorescent detection to identify small FRET changes will involve growing cultures to a lower OD_{600} than the tradition concentration of 1. Activity of the isolates also showed above basal fluorescence for GFP^2 (Figure 7A1), transfer Figure 7A2), and for $mRuby^2$ activity (Figure 7A3).

The library isolates utilized for all previous experiments were randomly chosen colonies to examine the basics of the system. Their fluorescent intensities were all quite low, with a few showing slightly brighter activity. To examine the variability and behavior of the entire library, cultures were grown and run on a 4 laser, 12 color LSR II flow cytometer (Kermit). Transfer activity was identified for the truncated library, slightly above negative controls (Figure 8A and 8B, green curve). The libraries also expressed similar GFP^2 activity above negative controls, however were significantly below positive control intensity (Figure 8C). Library peaks were not as broad for GFP^2 positive controls.

Once a positive clone is identified, it will be desired to sequence the plasmid to understand how the $mRuby^2$ was inserted into the third intracellular loop. Isolation of the plasmid and transfection into E. coli was attempted to prepare it for sequencing. A positive control strain (A4793), containing a plasmid with an ampicillin resistance (amp-R) gene was used to ensure that plasmid isolation and transfection were working. Two yeast miniprep kits were utilized, one enzymatic and one mechanical, to isolate the plasmid. Data is only shown for an extraction and transformation using the enzymatic protocol, the Zymolyase Miniprep kit. A nanodrop spectrophotometer confirmed the presence of nucleic acid between 25-35 ng/mL in the elutions from the miniprep kits. After transformation, the positive controls show significant colony growth, confirming isolation of plasmid from the yeast cells (Figure 9A and 9B). The negative control shows no growth, confirming the selective growth quality of the media (Figure 9C). Unexpectedly, all library isolates, truncated and full length, also showed no colony growth (Figure 9D). The plasmids used to create the libraries contain an amp-R gene which allows the E. coli to grow on the selective media. Multiple attempts of each protocol all yielded no E. coli growth from any library isolate of either L1858 or L1859.

To verify plasmid integrity, cultures were overgrown in YPD to allow for non-selective growth and to promote plasmid loss. Cultures were also overgrown in SD-ura and plated in a similar fashion as a selective growth control. Around 500 cells from each culture were plated on YPD and SD-ura plates and colony growth was compared after incubation. Similar numbers of colonies grew on each plate, although YPD colonies were often slightly larger than those on SD-ura plates (Table 1, Figure 10A). Cultures grown in YPD were then plated on YPD were then replica plated, using short fiber velveteen, onto FOA plates to select for colonies lacking uracil. After incubation, similar colony establishment and growth was seen between the YPD and FOA plates (Figure 10B).

As plasmid isolation proved to be difficult, colony PCR was identified as a possible option to get a product to sequence the IC3 mRuby^2 construct. Primers were used that flanked the IC3, in the transmembrane regions. Fresh plates were grown of negative mRuby^2 controls, A1239, A4242, and A4243, as well as isolates from both libraries. PCR was completed using the maximal number of recommended cycles and times for each step to optimize product yields; products were then run on a 0.9% agarose gel and imaged (Figure 11). Extremely faint bands can be seen for all four library isolates around 1000 kb as expected for an IC3 loop containing mRuby^2. All lanes show intense bands around 100 kb, the size of the wild type Ste2 IC3 loop. The negative control, A1239, which does not contain STE2 within the genome or on a plasmid, also showed an intense band here. These bands could be caused by primer oligomerization to each other and not from a positive Ste2 IC3 identification.

Discussion

A simplified version of the mammalian GPCR system can be found in the Ste2p receptor, a member of the yeast pheromone response mating pathway. Identification of Ste2p activation currently relies on downstream reporter gene transcription changes. A direct, immediate indicator is required for further understanding the interplay between agonist binding, receptor activation, and cellular response. Successful in other GPCRS, a FRET based system was developed for the Ste2p receptor.

A direct activation indicator system was developed in the Ste2p receptor, utilizing GFP^2 and $mRuby^2$ as the Förester pair. The spectra for each fluorophore were measured to help optimize excitation and detection for the system (Figure 6). Significant fluorescent activity was identified for $mRuby^2$ throughout flow cytometry analysis, however, the GFP^2 intensity was less remarkable. The presence of both fluorophores was confirmed within the receptor system (Figure 4, lanes have size expected for receptor and two fluorophores present). Detection of activity by flow cytometry was optimized using the measured spectra and machines available. Systems created in a receptor with a truncated c-terminal tail had significantly stronger fluorescent activity, identified by flow cytometry, for $mRuby^2$ but only slightly higher GFP^2 activity (Figure 2). Variation in $mRuby^2$ signaling intensity between isolates was also identified (Figure 3), indicating variation within the libraries. Once a positive isolate is identified, sequencing of the plasmid will be desired to locate the $mRuby^2$ within the IC3 loop to understand the proximity to GFP^2. Isolation of the plasmid and transformation into E. coli before sequencing could not be completed and raised questions about issues with plasmid integration or loss. Initial experiments have confirmed that the cells contain plasmids separate from the genomic DNA, however, issues with transformation into E. coli have not been resolved. Although issues with transformation exist, the plasmid is present and functional within the cells. Overall, the system has potential to identify conformational changes associated with ligand binding within Ste2p. A positive clone from the library will have strong fluorescence which will have a detectable change, by use of a flow cytometer, upon the induction of α-factor. Optimization of the construct is ultimately required if the system is to have the usability and functionality desired.

Spectral measurements were done to confirm peaks as limited literature was available for the fluorophores, especially when in yeast cells. Identification of the optimal

excitation of the fluorophores ensured production of the maximal output, while detection of this output was optimized by the emission spectra. Fluorimeter data also identified the impact from basal cell fluorescent signaling. Spectra were determined by subtracting out basal fluorescence from the cells and optimizing excitation to remove overlap of the machine's Raman peak from the fluorophore emission peak (Lawaetz & Stedmon 2009). Although the fluorimeter was useful to determine the fluorophore spectra, examining isolates and controls on a fluorimeter was time-consuming compound with the fact that scattering from excess cells, utilizing a stir bar to keep cells suspended, and media all caused significant noise during detection. Weak mRuby^2 signal over basal fluorescence also caused noise during analysis. Further experiments of varying concentrations of cells are needed to obtain the strongest signal possible while not compromising detection from scattering and noise. Fluorimeter experiments require cell suspensions in PBS for clean spectra, however, agonist binding is not efficient in this environment. Identification of FRET changes from activation would not be possible, or time effective, on a fluorimeter.

However, the use of a high-throughput flow cytometer allowed for efficient and accurate screening of the libraries. Detection was not impacted by the use of SD-ura (Supplementary Figure 1) because, unlike in the fluorimeter, cells are individually excited and examined in the flow cell of the cytometer. Multiple cytometers were available, from the URMC flow core; the optimal excitation and detection for the system was examined by using multiple machines. Collectively, similar trends were seen from the receptor system on all machines: strong mRuby^2 activity with low levels of GFP^2 or transfer fluorescence present. The c-terminally truncated receptors consistently expressed strong fluorescent activity, as predicted. Truncated receptors do not get internalized and degraded as quickly, and a higher concentration of receptors lead to a strong fluorescent signal. Often, the full length receptors exhibited fluorescent activity only slightly above basal signaling. Increasing full length receptor concentrations at the surface could improve their fluorescent output.

High throughput screening of the entire library to find brighter than average isolates is the next step in identifying a positive clone. The initial run of the entire library showed some variation in the library, however peaks were not extremely broad. Possible transfer activity (Figure 8A and 8B) was identified, however, this signal could be a false

positive. Excitation at 488 nm could be exciting mRuby^2, although the truncated library signal is greater than the positive mRuby^2 control. The difference in fluorescent intensities for the libraries above negative controls is not noteworthy. Sorting the library for isolates that express stronger fluorescent intensities may make these differences and future FRET changes easier to identify. However, sorting the library for strictly bright clones decreases genetic diversity and therefore the chance of finding a receptor construct that responds to ligand binding to produce a differential FRET output. This is a limiting factor that could be eliminated by increasing the overall fluorescent output of the entire system. Sorting for brighter isolates by the flow cytometer must also be corrected for doublet false signals. When two cells enter the flow cell simultaneously they will both emit a signal together, however, the cytometer will include these doublets in the positive sort. Gating is possible to eliminate the doublets from analysis through comparing the forward and side scattering (Supplementary Figure 2). High throughput screening and sorting will also be used to identify isolates with changes in fluorescent behavior upon induction of ligand and this gating will be necessary to eliminate false positives. Stringent gating and resorting of large numbers of cells will be required to find a positive isolate from the entire library. High throughput sorting allows for a random mutagenesis approach inserting mRuby2 into the IC3 to create a large, diverse library that most likely contains a positive isolate.

In a positive clone, a successful construct would identify differential fluorescent intensity upon ligand binding. For the isolates randomly chosen to ensure the system was functional, none exhibited a change in fluorescence upon induction with α-factor (Supplementary Figure 3). There were minor changes in fluorescent activity, however, it needs to be determined a significant shift is. It is possible that the receptor is experiencing conformational changes, however they are not inducing FRET changes because the fluorophores are in too close proximity. Little GFP^2 fluorescent activity was identified throughout screening, which may be caused by complete quenching of all energy by the mRuby^2 acceptor fluorophore. Determined by the properties of the fluorophores used, maximal efficiency of energy transfer can occur even if the proteins are not touching, but in close enough proximity. Although truncated isolates displayed significantly brighter fluorescence over full length isolates, the shortened c-tail may not be long enough to allow for enough distance between fluorophores for detectable changes in FRET activity. Optimal detection of changes occurs when energy transfer

efficiency is around 50%, as even small distances can create significantly different fluorescent outputs (Supplementary Figure 4).

Once a positive clone is identified through screening of the entire libraries, sequencing of the third intracellular loop will be desired to understand the placement and proximity of mRuby^2 to GFP^2. Initial isolation of the plasmid and transformation into E. coli for amplification before sequencing was not successful. DNA presence was confirmed within elutions through a nanospec, however this could be entirely genomic which would be unable to allow E. coli growth on selective media. To ensure the plasmid is present, elutions could be run on an agarose gel to identify DNA of the correct projected length of the plasmid. An interruption of the amp-R gene is the most likely explanation of the failure to have colony growth. It is unlikely that mutagenesis caused this issue, as every isolate attempted was not successful. If addition of mRuby^2 caused a shift in the plasmid, only a small population of plasmids would not be successful for transformation. This hypothesis could be tested by attempting transformation with a GFP^2 control (A4242 or A4243). If transformation is successful, it can be inferred that mutagenesis disrupted the plasmid amp-R gene. It was speculated that the plasmid did not exist separate from the genomic DNA, however the well-studied background strain used to develop the libraries not before had this issue. FOA plating confirmed that plasmid loss was possible, as colony growth was established when uracil becomes a lethal selective measure (Figure 10). Although not resolved, this issue can be bypassed and sequencing is still possible. The variable region of plasmids between library isolates is contained to the mRuby^2 position within the IC3. Colony PCR utilizing primers flanking the IC3 can amplify this region of interest, products can be run on an agarose gel, and bands can be collected for sequencing (Supplementary Figure 5). PCR reactions must be large enough to produce intense bands to ensure enough product is available for collection. Further work is needed to identify the factor responsible for plasmid issues, however, a positive clone can still be identified before this is resolved.

To improve versatility of the indicator system, it would be beneficial if the receptor was functional and induced a cellular response upon activation. Previous experiments have found only full length receptors are functional after insertion into the third intracellular loop (Mathew et al 2012). As the full length library had consistently low fluorescent activity, finding a functional receptor that also has a strong enough signal to identify

FRET changes poses an issue. Truncated receptor constructs experience increased receptor localization to the membrane, which is also possible for full length isolates through substitution of the seven lysine in the c-terminal tail to arginine (Ballon et al 2006). Increased concentrations of receptors at the surface should improve fluorescent output. A significant issue within the full length receptors, as identified by the Western blot, was GFP^2 cleavage off of the system. This was also confirmed by the large localization of fluorescent intensity within the cell (Figure 5A). Moving the system into a new strain, one without proteolytic activity, may help increase signal output as well. If a positive clone is identified in the current system, it can easily be improved by these methods. Or, the system can be redesigned to incorporate these and other enhancements.

Currently, this system is built as a multi-copy plasmid expressing maximal numbers of receptors. However, projected studies with this indicator system rely on varying concentrations of receptors to understand behavior (Rajashri et al 2016). Increasing fluorescent output as indicated above, in the current system, may still not be enough to utilize single copy plasmids. Other FRET-based indicator systems have been successful in other GPCRs, however, these systems often utilize small fluorescent reagents or bioluminescent molecules. The use of two fluorescent proteins has caused issues for functionality because of the bulk introduced into the receptor. Utilizing a FlAsH/FRET combination may be a beneficial change for this receptor construct. Introducing a small sequence into the IC3, which binds to a small organic fluorescent molecule as done for FlAsH, has been shown not to impair the functionality of tagged receptors (Hoffmann et al 2005). This technique also results in stronger fluorescent signals, which could increase the possibility of developing a successful full length receptor construct. Another major issue experienced by FRET systems is a result of excessive spectral overlap creating a false positive of transfer activity (reviewed by Kauk & Hoffman 2018). It is possible that signals believed to be transfer activity (Figure 8) could be a result of GFP^2 signal bleeding into $mRuby^2$ detection, or slight excitation of $mRuby^2$. Optimization of the indicator system relies on utilizing the best aspects of all techniques to produce a distinct FRET signal that responses to conformational changes induced by ligand binding.

A functional indicator system would allow further studies of receptor behavior and signaling output. The dynamic relationship between ligand binding, receptor activation, and cellular response is the basis of the dosage curve for GPCR targeted pharmaceuticals. Utilizing this activation indicator can further research understanding the idea of fractional occupancy and other receptor behaviors. A vital element of furthering research would include using this indicator with varying concentrations of receptors, however fluorescent intensity must be increased if this is to be possible. Current behavior and mechanisms of Ste2p are only partially understood. Understanding response outputs from ligand binding and receptor activation will allow the pharmaceutical field to better target and dose GPCR medications. GPCRs are present throughout the body and are the target of over one third of the drugs on the market today. The importance of GPCR research cannot be understated.

Conclusions

The development of a successful FRET-based indicator system is possible and a positive clone could be identified from the current library construct. However, multiple improvements are possible and should be utilized to create a functional and versatile construct, such as the use of FlAsH reagents. Activation sensors have been developed in other GPCRs that utilize these improvements. Further sorting of the library could lead to the detection of a positive clone that displays changes in fluorescent activity upon the binding of ligands. A functional indicator of Ste2p activation can further research to understand the dynamic relationship between ligand binding, receptor activation, and cellular response output.

Appendix:

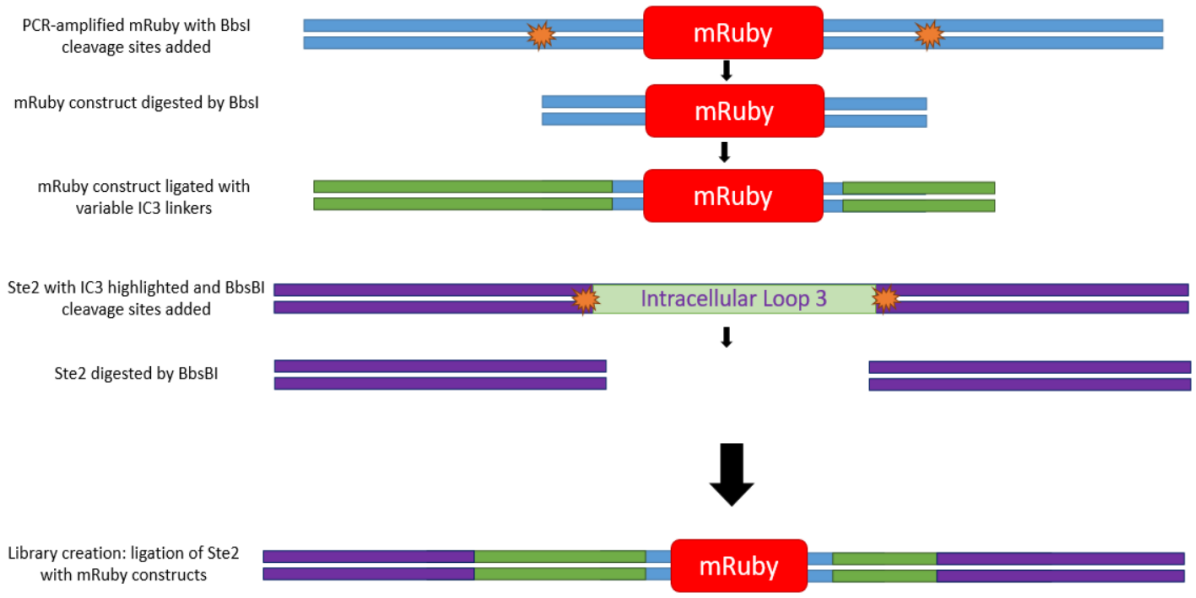

Figure 1: Schematic of the protocol used to create mutant libraries of Ste2, with mRuby^2 inserted into the IC3 loop region with variable length linkers, as adapted from Mathew et al 2012

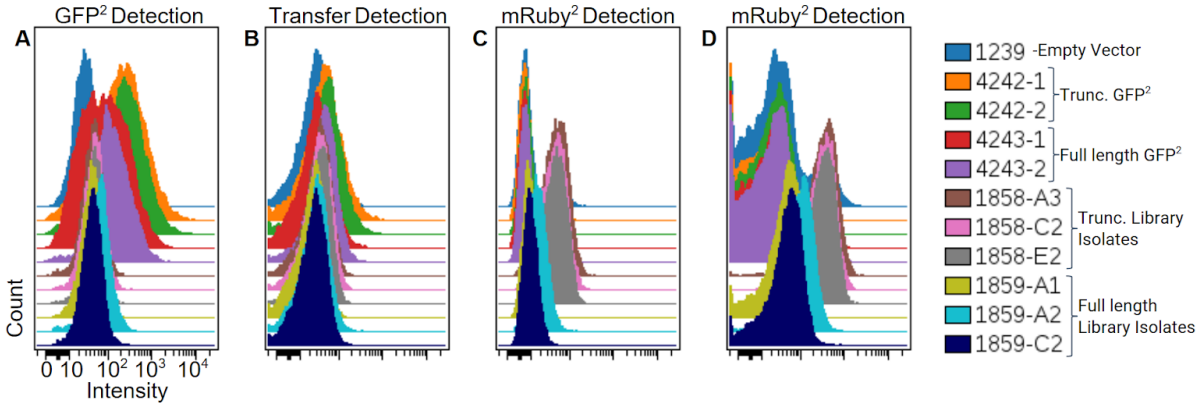

Figure 2: Initial flow run of randomly selected isolates, mean fluorescent intensity on logarithmic scale: A. GFP^2 detection, Violet E (405 nm excitation, detector 525/50 nm bandpass) B. Transfer energy detection, Violet D (405 nm excitation, detector 610/20 nm bandpass) C. mRuby^2 detection, YG E (561 nm excitation, 586/15 nm bandpass detection) D. mRuby^2 detection, YG D (561 nm excitation, 610/20 bandpass detection)

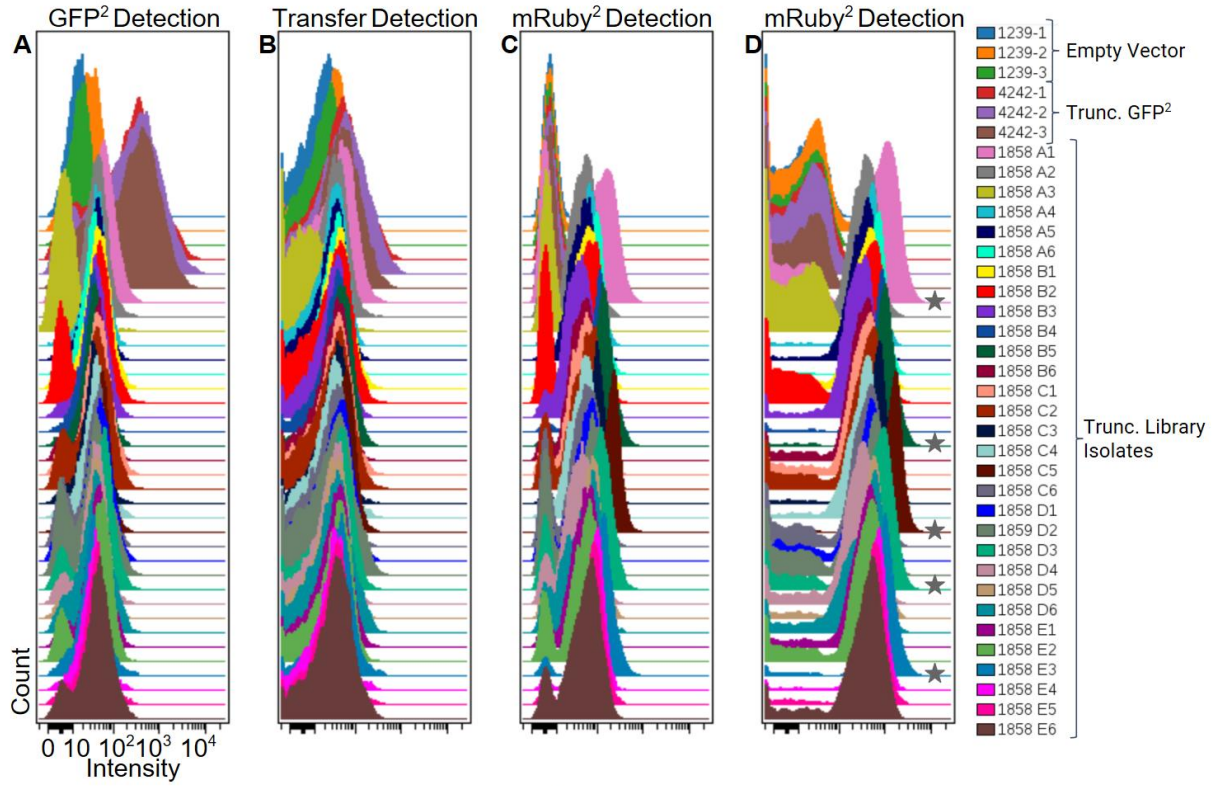

Figure 3: Randomly chosen truncated isolates to identify GFP² and transfer activity, mean fluorescent intensity on logarithmic scale: A. GFP² detection, Violet E (405 nm excitation, detector 525/50 nm bandpass) B. Transfer energy detection, Violet D (405 nm excitation, detector 610/20 nm bandpass) C. mRuby² detection, YG E (561 nm excitation, 586/15 nm bandpass detection) D. mRuby² detection, YG D (561 nm excitation, 610/20 bandpass detection), stars indicate brighter than average isolates.

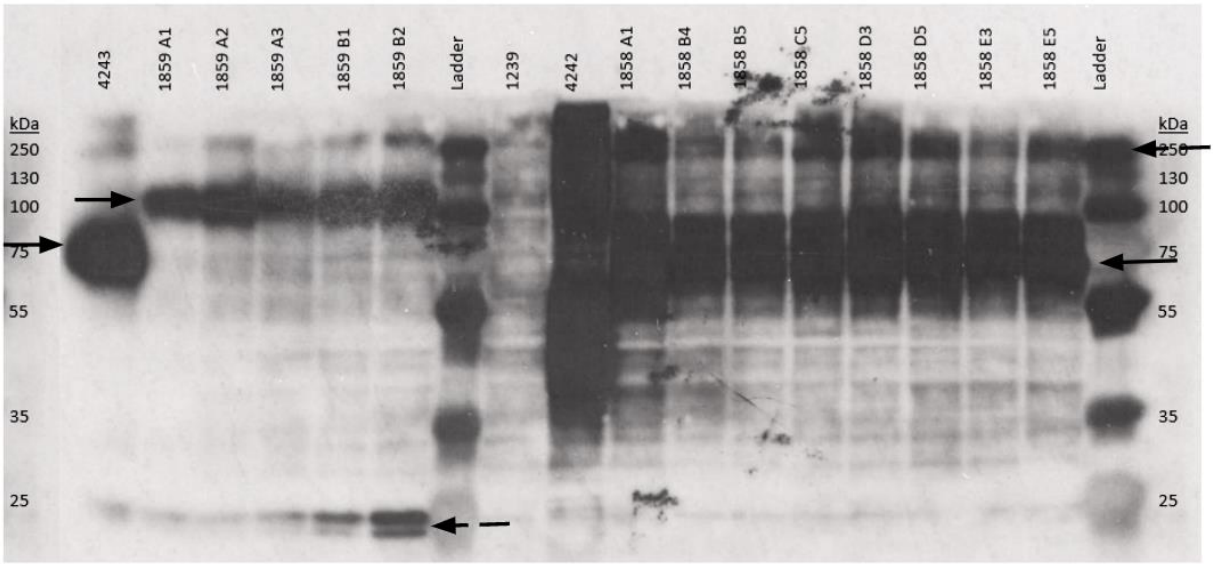

Figure 4: Western Blot of L1859 and L1858 isolates using mouse anti-GFP antibody and goat anti-mouse HRP for detection; Full length control 4243 in lane 1, Empty vector control 1239 in lane 8, and truncated control 4242 in lane 9. Arrows indicate projected Ste2p construct locations, dashed arrows indicate cleavage or oligomerization.

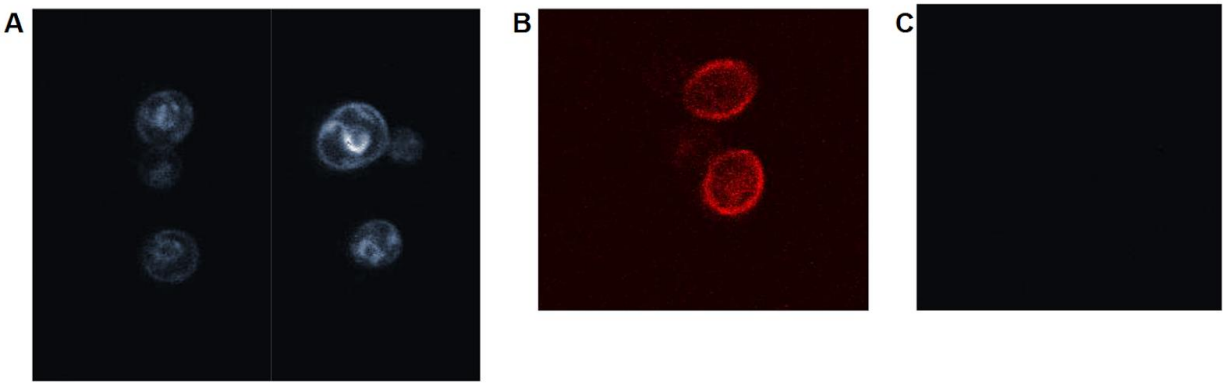

Figure 5: Confocal Microscopy imaging: A. A4242 showing GFP[2] activity and localization to membrane and in lysosome B. A5119 control showing mRuby[2] activity C. Isolate from L1858 showing no GFP[2] activity and expressing slight mRuby[2] activity (unable to image due to photobleaching)

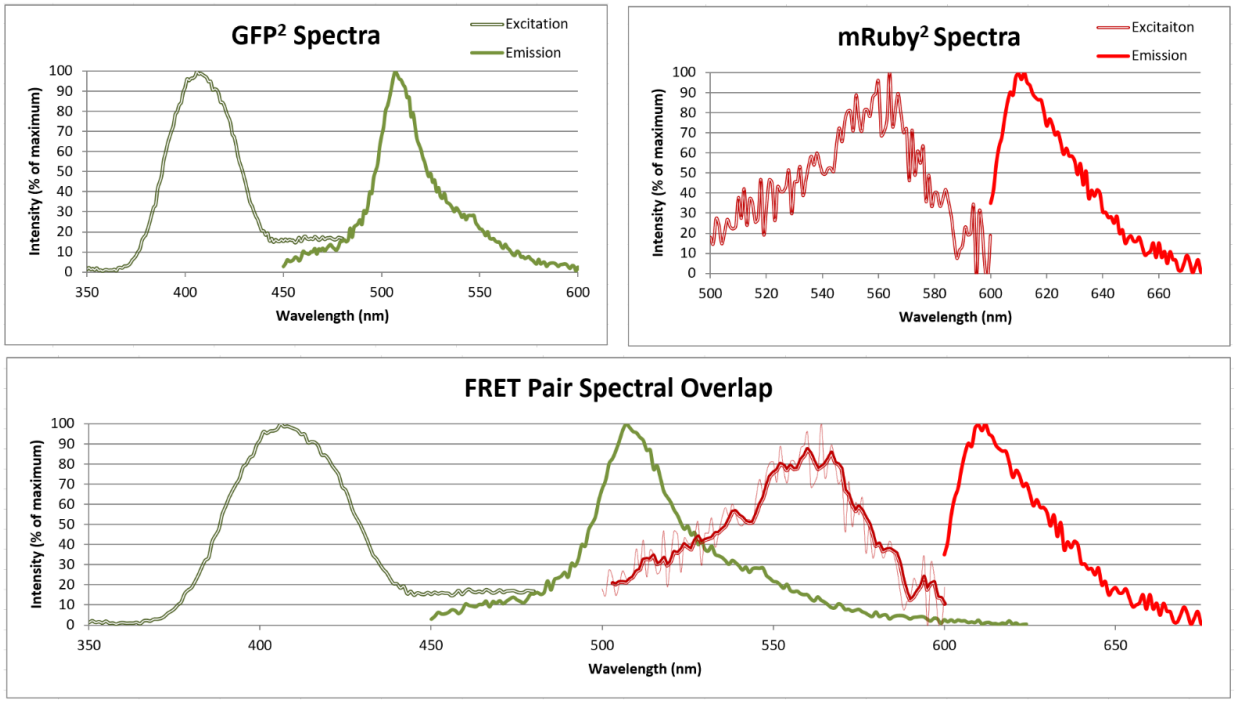

Figure 6: Spectra of fluorophores and spectra overlap of the FRET pair: A.GFP[2] spectra: excitation measured using 518 nm emission, emission measured using 420 nm excitation B. mRuby[2] spectra: excitation measured using 620 nm emission, emission measured using 564 nm excitation C. FRET pair spectral showing significant overlap predicted from around 475 nm to 600 nm, trendline with moving average used for mRuby[2] excitation to reduce noise

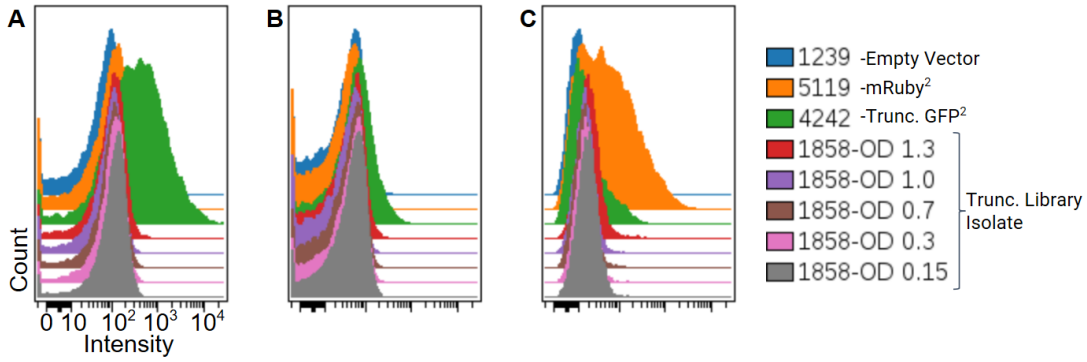

D

	GFP² Detection	Transfer Detection	mRuby² Detection
1239	713.7	372.6	96.9
5119	888.75	357.3	456.47
4242	3275.55	581.85	132.05
1858-OD 1.3	965.7	405.0	186.2
1858-OD 1.0	876.6	351.9	142.5
1858-OD 0.7	966.6	421.2	136.32
1858-OD 0.3	1032.3	459.0	153.9
1858-OD 0.15	1120.5	478.8	173.85

Figure 7: Truncated Growth Array, mean fluorescent intensity on logarithmic scale: A. GFP² detection, Violet G (407 nm excitation, detector 550/40 nm bandpass) B. Transfer energy detection, Violet C (407 nm excitation, detector 660/40 nm bandpass) C. mRuby² detection, Green D (530 nm excitation, 610/20 nm bandpass) D. Raw mean values of fluorescent intensity showing increasing values for decreasing optical density

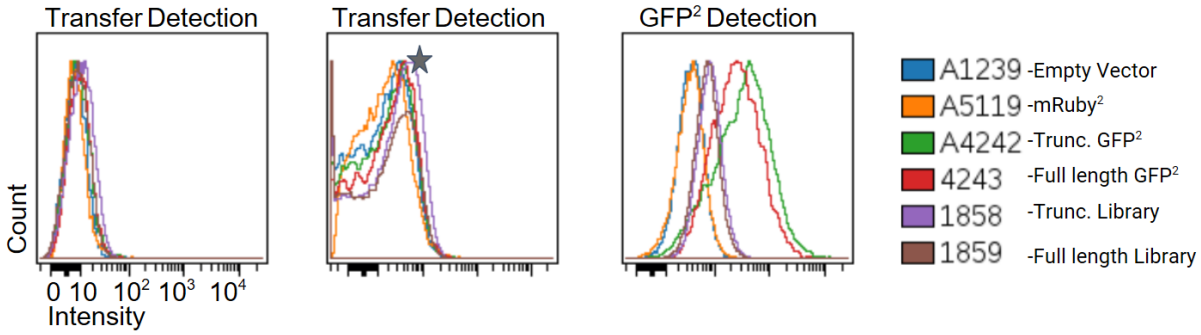

Figure 8: Full library examination, mean fluorescent intensity on logarithmic scale: A. Transfer energy detection, Blue D (488 nm excitation, detector 610/20 nm bandpass) B. Transfer energy detection, Blue C (488 nm excitation, detector 660/20 nm bandpass) C. GFP² detection, Violet B (407 nm excitation,525/50 nm bandpass)

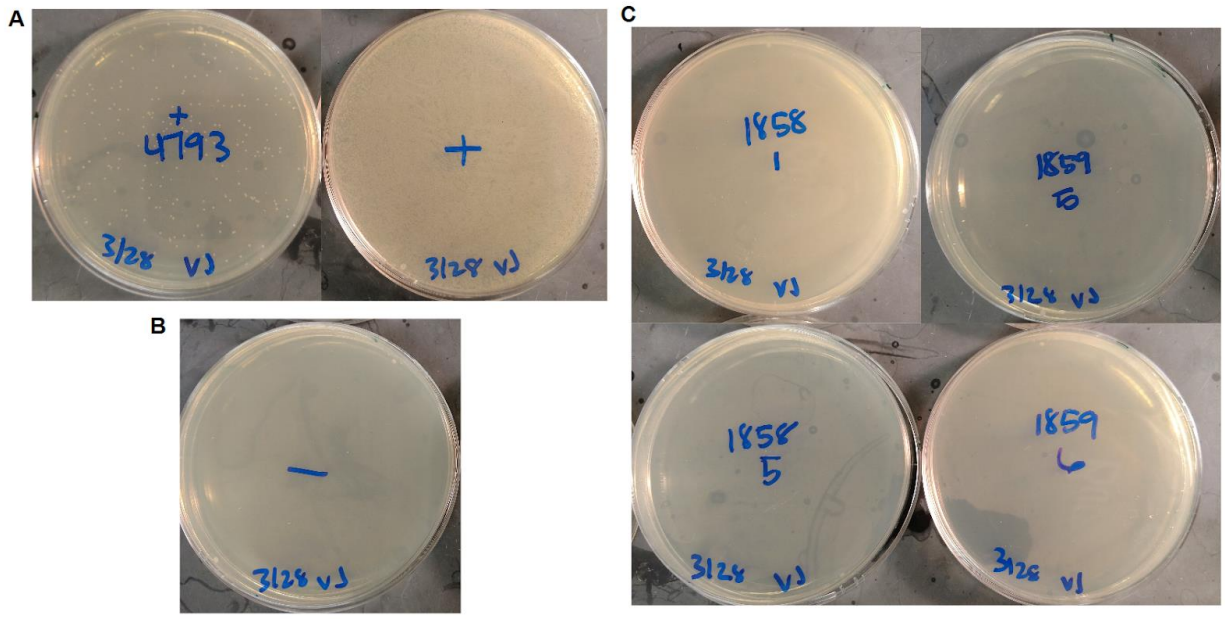

Figure 9: Transformation Results, Zymolyase Miniprep kit utilized: A. Positive extraction (A4793) and transformation (+) controls exhibit extensive colony growth B. Negative (-) transformation control verifying media is amp-R selective C. Truncated and full length library isolates exhibiting no colony growth after transformation with miniprep elutions

Liquid Media:	**YPD**		**SD-ura**	
Plated Media:	YPD	SD-ura	YPD	SD-ura
1858-1	92	100	101	110
1858-5	108	80	87	125
1859-1	97	89	115	90
1859-5	108	97	93	85

Table 1: Number of colonies in 1/6th sector of each plate after incubation at 37°C for 48 hours using randomly chosen truncated isolates (1858) and two randomly chosen full length isolates (1859)

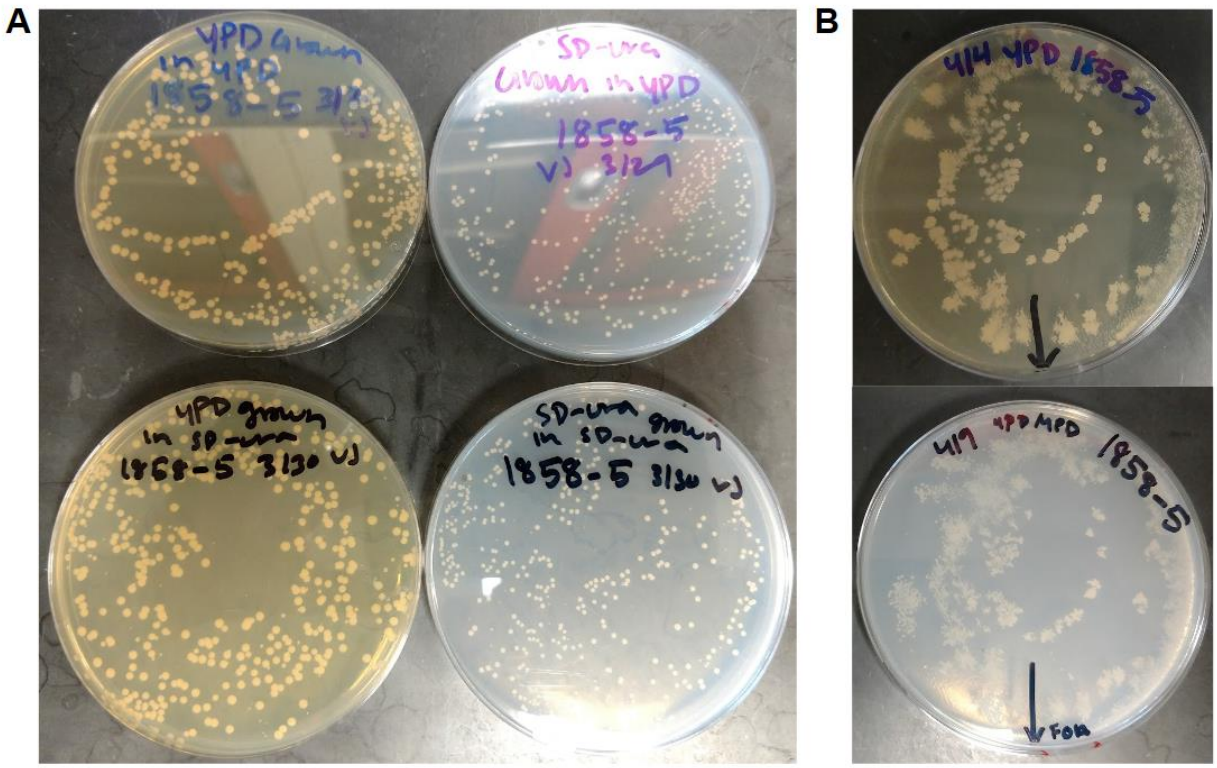

Figure 10: Ensuring plasmid vitality: A. Top row overgrown in YPD media, bottom row overgrown in SD-ura, left column YPD plated, right column SD-ura plated: Similar numbers of colonies on each plate, however YPD plated colonies are larger; similar trends are seen for other isolates B. Replica plating of colonies overgrown in YPD, plated on YPD onto FOA plates: Colony growth is evident on FOA restrictive media

Supplemental Figures:

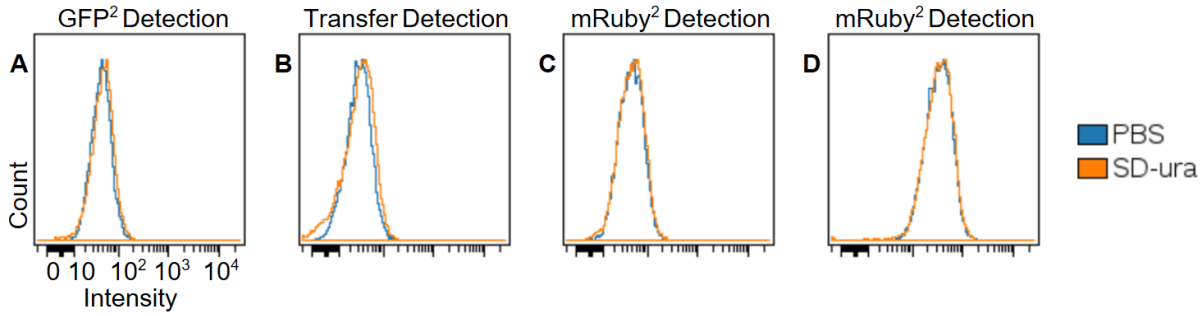

Supplemental Figure 1: Detection by flow cytometry in different medias: no major differences between SD-ura and PBS A. GFP^2 detection, Violet E (405 nm excitation, detector 525/50 nm bandpass) B. Transfer energy detection, Violet D (405 nm excitation, detector 610/20 nm bandpass) C. mRuby^2 detection, YG E (561 nm excitation, 586/15 nm bandpass detection) D. mRuby^2 detection, YG D (561 nm excitation, 610/20 bandpass detection)

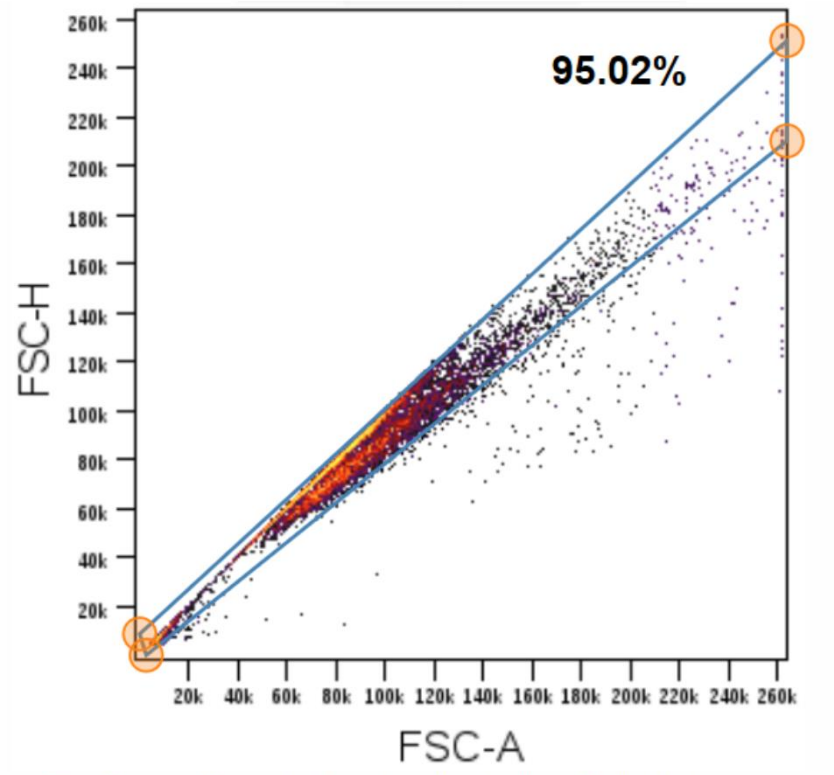

Supplemental Figure 2: Sample gating to eliminate doublet detection from sorting and analysis using forward side scattering (FSC) area plotted against FSC height

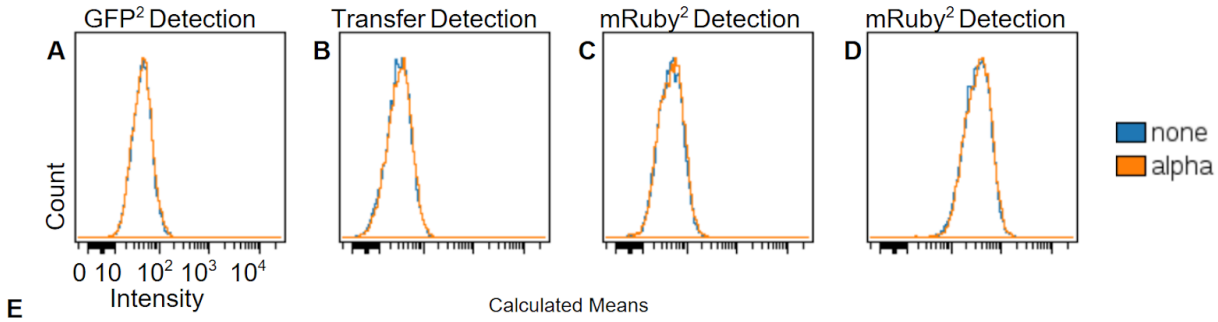

E

Calculated Means

none	478.57	340.66	518.49	3676.49
alpha	491.69	355.0	537.16	3804.16

Supplemental Figure 3: Changes in fluorescent intensity upon α-factor induction: no significant trends identified A. GFP² detection, Violet E (405 nm excitation, detector 525/50 nm bandpass) B. Transfer energy detection, Violet D (405 nm excitation, detector 610/20 nm bandpass) C. mRuby² detection, YG E (561 nm excitation, 586/15 nm bandpass detection) D. mRuby² detection, YG D (561 nm excitation, 610/20 bandpass detection) E. Calculated mean intensity values for each peak, all values increase 3-4%

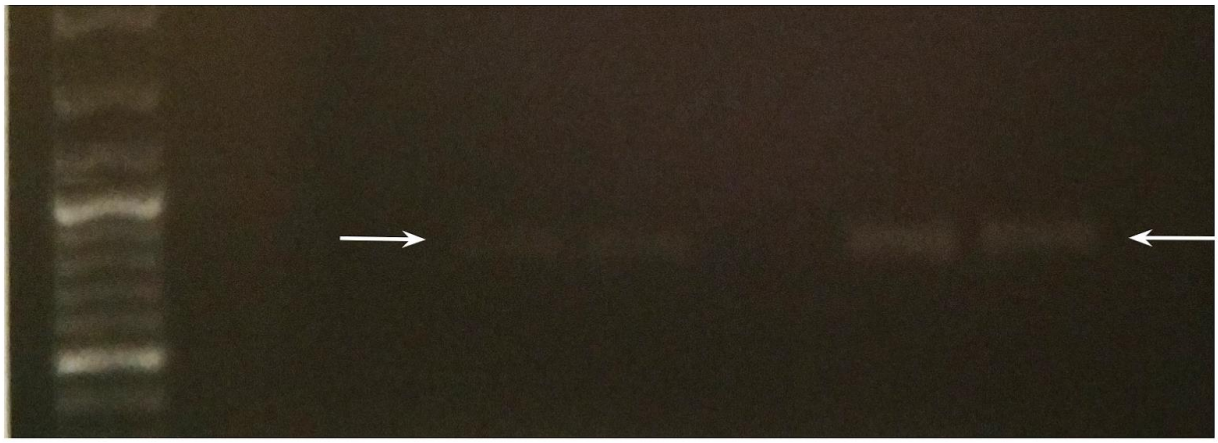

Supplemental Figure 4: Colony PCR products run on 0.9% agarose gel, arrows indicate extremely faint bands at 1,000 kb in lanes 3, 4, 6, and 7. Larger reactions of PCR are necessary for more intense bands and then collection for sequencing.

References

Ballon, B. et al. (2006) DEP-Domain-Mediated Regulation of GPCR Signaling Responses, *Cell,* 126, pages 1079-1093.

Bardwell, L. (2004) A walk-through of the yeast mating pheromone response pathway, *Peptides,* 25, pages 1465-1476.

Bosier, B. and Hermans, E. (2007) Versatility of GPCR recognition by drugs: from biological implications to therapeutic relevance, *Trends Pharmacol Sci,*

Bünemann, M., Frank, M., Lohse, M., (2003). Gi protein activation in intact cells involves subunit rearrangement rather than dissociation, *PNAS*, 100, pages 16077-16082.

Bush, A. et al. (2016) Yeast GPCR signaling reflects the fraction of occupied receptors, not the number, *Mol Syst Biol,* 12, pages 1-12.

Cevheroğlu, O. et al. (2017) The yeast Ste2p G protein-coupled receptor dimerizes on the cell plasma membrane, *BBA-Biomembranes,* 1859, pages 698-711.

Cevheroğlu, O., Becker, J., and Son, Ç. (2017) GPCR-Gα protein precoupling: Interaction between Ste2p, a yeast GPCR, and Gpa1p, its Gα protein, is formed before ligand binding via the Ste2p C-terminal domain and the Gpa1p N-terminal domain, *BBA-Biomembranes,* 1859, pages 2435-2446.

Fredriksson, R. and Schiöth, H. (2005) The Repertoire of G-Protein-Coupled Receptors in Fully Sequenced Genomes, *Mol Pharmacol,* 67, pages 1414-1425.

Gehret, A., Connelly, S., and Dumont, M. (2012) Functional and Physical Interactions among Saccharomyces cerevisiae α-Factor Receptors, *Eukaryot Cell,* 11, 1276-1288.

Goffeau, A. et al. (1996) Life with 6000 Genes, *Science*, 274, pages 546, 563-567.

Gutierrez, A. and McDonald, P. (2018) GPCRs: Emerging anti-cancer drug targets, *Cell Signal,* 41, pages 65-74.

Hein, P. and Bünemann, M. (2009) Coupling mode of receptors and G proteins, *Naunyn-Schmied Arch Pharmacol,* 379, pages 435-443.

Hoffman, C. et al. (2005) A FlAsH-based FRET approach to determine G protein-coupled receptor activation in living cells, *Nature Methods,* 2, pages 171-176.

Insel, P. et al. (2007) Impact of GPCRs in clinical medicine: Monogenic diseases, genetic variants and drug targets, *Biochim Biophys Acta,* 1786, pages 994-1005.

Kam, A. et al. (2012) Improving FRET dynamic range with bright green and red fluorescent proteins, *Nature Methods,* pages 1005-1012.

Kauk, M. and Hoffman, C. (2018) Intramolecular and Intermolecular FRET Sensors for GPCRs-Monitoring Conformational Changes and Beyond, *Trends Pharmacol Sci*, 39, pages 123-135.

Kenakin, T. (2007) Functional Selectivity through Protean and Biased Agonism: Who Steers the Ship?, *Mol Pharmacol,* 72, pages 1393-1401.

Kim, K-M. et al. (2011) Multiple regulatory roles of the carboxy terminus of Ste2p a yeast GPCR, *Pharmacol Res,* 65, pages 31-40.

Kobilka, B. (2007) G Protein Coupled Receptor Structure and Activation, *Biochim Biophys Acta,* 1768, pages 794-807.

Kredel, S. et al. (2009) mRuby, a Bright Monomeric Red Fluorescent Protein for Labeling of Subcellular Structures, *PLoS One*, 4, pages 1-7.

Lawaetz, A. and Stedmon, C. (2009) Fluorescence Intensity Calibration Using the Raman Scatter Peak of Water, *Appl Spectrosc,* 63, pages 936-940.

Liu, R. et al. (2016) Human G protein-coupled receptor studies in Saccharomyces cerevisiae, *Biochem Pharmacol,* 114, pages 103-115.

Mathew, E. et al. (2013) Functional fusions of T4 lysozyme in the third intracellular loop of a G protein-coupled receptor identified by a random screening approach in yeast, *Protein Eng Des Sel*, 26, pages 59-71.

Rask-Andersen, M., Almen, M., and Schioth, H., Trends in the exploitation of novel drug targets, *Nature Rev Drug Disc,* 10, pages 579-590.

Rosenbaum, D., Rasmussen, S., and Kobilka, B. (2009). The structure and function of G-protein-coupled receptors, *Nature,* 459, pages 356-363.

Sridharan, R. et al. (2013) Fluorescent approaches for understanding interactions of ligands with G protein coupled receptors, *Biochim Biophys Acta,* 1838, pages 15-33.

Sridharan, R. et al. (2016) Variable Dependence of Signaling Output on Agonist Occupancy of Ste2p, a G Protein-coupled Receptor in Yeast, *J Biol Chem*, 291, pages 24261-24279.

Tang, X. et al. (2012) Orphan G protein-coupled receptors (GPCRs): biological functions and potential drug targets, *Acta Pharmacol Sin,* 33, pages 363-371.

Taslimi, A. et al. (2012) Identifying Functionally Important Conformational Changes in Proteins: Activation of the Yeast α-factor Receptor Ste2p, *J Mol Biol,* 418, pages 367-378.

Uddin, M. et al. (2016) The N-terminus of the yeast G protein-coupled receptor Ste2p plays critical roles in surface expression, signaling, and negative regulations, *Biochim Biophys Acta,* 1858, paes 715-724.

Yan, Y-X. et al. (2002) Cell-Based High-Throughput Screening Assay System for Monitoring G Protein-Coupled Receptor Activation Using β-Galactosidase Enzyme Complementation Technology, *J Biomol Screen,* 7, pages 451-460.

Zimmermann, T. et al. (2002) Spectral imaging and linear un-mixing enables improved FRET efficiency with a novel GFP2-YFP FRET pair, *FEBS Lett,* 531, pages 245-249.